Journal of Power Sources 216 (2012) 208–215

Contents lists available at SciVerse ScienceDirect

Journal of Power Sources

journal homepage: www.elsevier.com/locate/jpowsour

$Sm_{0.5}Sr_{0.5}CoO_{3-\delta}$-infiltrated cathodes for solid oxide fuel cells with improved oxygen reduction activity and stability

Fucun Wang, Dengjie Chen, Zongping Shao*

State Key Laboratory of Materials-Oriented Chemical Engineering, College of Chemistry & Chemical Engineering, Nanjing University of Technology, No. 5 Xin Mofan Road, Nanjing 210009, PR China

HIGHLIGHTS

- $Sm_{0.2}Ce_{0.8}O_{1.9}$ (SDC) was preferred as a porous scaffold for the infiltration.
- A pure $Sm_{0.5}Sr_{0.5}CoO_{3-\delta}$ (SSC) phase was formed with glycine as a complexing agent.
- Electrical conductivities of ~15 S cm^{-1} were achieved with 20 wt% SSC + 80 wt% SDC.
- A stable performance was obtained with a 20 wt% SSC + 80 wt% SDC electrode.
- A 20 wt% SSC + 80 wt% SDC electrode showed a resistance of 0.05 Ω cm^2 at 700 °C.

ARTICLE INFO

Article history:
Received 20 April 2012
Received in revised form
22 May 2012
Accepted 23 May 2012
Available online 30 May 2012

Keywords:
Solid oxide fuel cells
Cathodes
Infiltration
Long-term stability

ABSTRACT

$Sm_{0.5}Sr_{0.5}CoO_{3-\delta}$ (SSC)-impregnated cathodes are fabricated by the solution infiltration of metal nitrates. The effects of complexing agents on the phase structure and the effects of pore formers on the porosity of the scaffold are examined and optimized. The thermal expansion behavior, electrical conductivities and electrochemical performance of the cathodes are characterized and optimized. A pure perovskite phase is formed after heating at 800 °C by adding a relatively small quantity of glycine as the complexing agent. Polyvinyl butyral is selected as the pore former for the preparation of porous $Sm_{0.2}Ce_{0.8}O_{1.9}$ (SDC) scaffolds. The thermal expansion coefficient increases slightly from 12.74×10^{-6} K^{-1} to 13.28×10^{-6} K^{-1} after infiltrating 20 wt% SSC into the SDC scaffold. The infiltrated cathode with 20 wt% SSC + 80 wt% SDC shows the electrical conductivity of 15 S cm^{-1} at 700 °C. A well-connected SSC network is formed in the cathode after infiltrating 20 wt% SSC into the SDC scaffold. Cathode polarization resistance values as low as 0.05 Ω cm^2, peak power density values as high as 936 mW cm^{-2} and stable performance throughout 325 h of operation at 700 °C suggest that the cathodes with the 20 wt% SSC-infiltrated SDC are suitable for practical application. However, for the SSC infiltrated into the 8 mol% yttria-stabilized zirconia scaffold, the interfacial reaction continues to occur during the stability test at 700 °C. SDC is preferred as a scaffold for the infiltration of SSC to ensure long-term operational stability.

1. Introduction

Solid oxide fuel cells (SOFCs), which are among the cleanest and most efficient electrochemical energy conversion devices, have been recognized as potential power sources to meet a quickly expanding energy demand without the environmental pollution created by conventional technologies [1]. Much effort is currently being expended to develop SOFCs into practical devices. Lowering their operating temperature to an intermediate range, 500–800 °C, is believed to be the key to promote the commercialization of SOFCs technology because it would effectively reduce the operating cost and prolong the operating lifetime [2–4]. Unfortunately, a polarization loss at the state-of-the-art $La_{0.8}Sr_{0.2}MnO_3$ cathode increases sharply with a reduction in the operating temperature. This polarization loss contributes to the overall energy loss and results in an unaffordable power output from the cells.

Because the oxygen reduction activity of the SOFCs cathodes is closely related to the material composition, considerable research efforts are ongoing to develop new cathode materials to increase the reduced-temperature performance [5]. Cobalt-containing perovskite oxides with mixed oxygen ionic and electronic conductivity have recently attracted attention; among them, $Sm_{0.5}Sr_{0.5}CoO_{3-\delta}$ (SSC), which possesses extremely high electrical conductivity and rapid oxygen surface exchange kinetics at elevated temperatures, is one of the most widely studied [6,7]. Results found in the literature have demonstrated that the SSC cathode possesses electrocatalytic activity favorable for an oxygen

* Corresponding author. Tel.: +86 25 83172256; fax: +86 25 83172242.
E-mail address: shaozp@njut.edu.cn (Z. Shao).

0378-7753/$ – see front matter © 2012 Elsevier B.V. All rights reserved.
doi:10.1016/j.jpowsour.2012.05.068

reduction reaction (ORR) at reduced temperatures [8–12]. However, two factors prevent SSC from performing effectively as a cathode in SOFCs: a mismatch of thermal expansion with other cell components and its easy reaction with the state-of-the-art stabilized zirconia electrolytes during its high-temperature fabrication [6]. The thermal expansion coefficient (TEC) of SSC is $\sim 24 \times 10^{-6}$ K^{-1} [6], much larger than those of commonly used electrolytes such as $\sim 10 \times 10^{-6}$ K^{-1} for 8 mol% yttria-stabilized zirconia (YSZ) [13] and $\sim 12 \times 10^{-6}$ K^{-1} for $Sm_{0.2}Ce_{0.8}O_{1.9}$ (SDC) [14]. The mismatch in thermal expansion between the cathode and the electrolyte may result in a slow delamination of the cathode layer from the electrolyte surface or the formation of cracks in the cathode layer due to the internal stress that emerges during long-term operation or during heating and cooling cycles. In addition, the unfavorable phase reaction between the components during their high-temperature fabrication will lead to the formation of a highly resistive interfacial layer at the interface of the cathode and the electrolyte, which can block oxygen ion transport, thus significantly deteriorating the cell performance. Cobalt-containing perovskite oxides have demonstrated high reactivity with the YSZ electrolyte at elevated temperatures.

Previous research has demonstrated that the problems associated with the thermal expansion mismatch and the serious phase reaction between the cell components may be moderately alleviated by the fabrication of a unique cathode structure consisting of a nano-structured cathode and a porous electrolyte scaffold through infiltration in connection with low-temperature sintering [15–19]. Furthermore, the nano-structured cathodes created via a metal salt solution infiltration possess a high surface area and significantly enhanced ORR kinetics, thus resulting in low interfacial polarization resistance [20]. However, nanoscale materials in the nano-structured cathode may have limited practical applications in SOFCs because the grain growth of nano-particles is expected to occur at the typical operating temperatures of SOFCs [21]. In addition, the potential phase reaction remains of great concern as the phase reaction between the cell components is a function not only of the sintering temperature but also the operating time. For example, an initial polarization resistance of 0.03 $\Omega\,cm^2$ was obtained with the $La_{0.6}Sr_{0.4}CoO_{3-\delta}$ (LSC)-infiltrated YSZ cathode, but the long-term cathode performance was unstable at an operating temperature of 700 °C [17]. This result suggests that a more detailed investigation of the infiltrated cathodes is still needed to realize their practical application. SDC has much better chemical compatibility with SSC than does YSZ. No chemical reaction occurs between SSC and SDC at temperatures higher than 1100 °C.

In the present study, we reported the fabrication and optimization of SSC-infiltrated cathodes for SOFCs with SDC and YSZ as electrolytes via solution infiltration. This research is of interest because of the high electrical conductivity and oxygen surface exchange kinetics of the SSC and because of the versatility of the solution infiltration technique. Two types of cathodes were prepared, a cathode with SSC infiltrated into a porous SDC scaffold and a cathode with SSC infiltrated into a YSZ scaffold. The effects of organic compounds on the formation of SSC perovskite and the properties and performance of the resulting cathodes were systematically studied. The fabrication parameters were also optimized. Emphasis was paid to the long-term stability of the two cathodes.

2. Experimental

2.1. Synthesis and fabrication

Nitrate raw materials (analytical reagent grade) were used to synthesize the SDC powder via a combined EDTA–citrate complexing method. A detailed procedure for the preparation of the SDC powder was reported in a previous publication [22]. Commercial products of YSZ (Tosoh, Tokyo, Japan, average particle size: 0.3 μm) and NiO (Shudu Nano-Science Development Co., Ltd., Chengdu, China, average particle size: 8 μm) were used in this experiment.

The disk-shaped pellets for the infiltration with the configuration of porous electrolyte/dense electrolyte/porous electrolyte were fabricated as follows: electrolyte pellets were first pressed uniaxially and sintered at 1450 °C for 5 h to ensure a relative density above 98%; then, proper SDC or YSZ and the 10 wt% (relative to the electrolyte powder and pore former) pore former (PVB, soluble starch or graphite) were mixed in a solution of glycerol, ethylene glycol and isopropyl alcohol using a high-energy ball mill (Fritsch, Pulverisette 6) at a rotational speed of 400 rpm for 0.5 h to form a slurry. This slurry was sprayed onto both surfaces of the electrolyte and sintered in air at 1300 °C for 5 h to form the porous electrolyte scaffolds. The thickness of the scaffolds is ~15 μm.

The SSC phase was prepared within the porous scaffolds by solution infiltration. The 0.8 mol L^{-1} SSC precursor solution used for the infiltration was prepared by dissolving $Sm(NO_3)_3 \cdot 6H_2O$, $Sr(NO_3)_2$ and $Co(NO_3)_2 \cdot 6H_2O$ at a molar ratio of Sm:Sr:Co = 0.5:0.5:1 with complexing agents and a surfactant in de-ionized water. Various complexing agents such as glycine, citric acid or urea were tested and the molar ratio of the complexing agent to the SSC was 2:1. Ethanol was reported to modify the liquid surface tension [23]; thus, it was added into the aqueous solution as the surfactant at a ratio of 1:3. A microliter syringe was used to infiltrate the solution into the porous scaffold for rough control of the SSC amount, while the precise infiltrated amount of SSC was analyzed using an electronic balance. The load of SSC can be calculated using the equation SSC% = mSSC/(mSSC + mSDC) × 100% in which mSSC and mSDC are the weights of the infiltrated SSC and the SDC scaffold, respectively. A vacuum apparatus and a hot plate (60 °C) were employed to remove gas from the micropores and force the liquid into the scaffold. The infiltration/firing steps were repeated until the desired amount of SSC was introduced. The infiltrated cathodes were finally calcined at 800 °C for 2 h to allow the formation of an SSC phase.

The anode-supported single fuel cell (Ni-YSZ/YSZ/SSC-infiltrated SDC) was fabricated to evaluate electrochemical performance in a real fuel cell. The Ni-YSZ anode substrate was prepared through a tape-casting process, and the thin-film YSZ electrolyte was prepared via wet powder spraying and co-sintering at 1450 °C for 5 h in air. The cathode was fabricated by the same infiltration method used to fabricate the symmetrical infiltrated cathodes.

To measure the electrical conductivity and thermal expansion behavior, rectangular bars with the dimensions of approximately 2 mm × 5 mm × 10 mm and the same porosity as the porous electrolyte scaffold were also prepared. Instead of infiltrating with a microliter syringe, the porous bars were steeped in an SSC solution. To introduce a desired amount of SSC, multiple infiltrations were required.

2.2. Characterization

The phase structure of the samples at room temperature was analyzed using powder X-ray diffraction (XRD) with a diffractometer (D8 Advance, Bruker) using Cu-Kα radiation (λ = 1.5418 Å) at 40 kV and 40 mA. The diffraction patterns were collected by step scanning in a 2θ range of 20–80° with the scan rate of 10°min^{-1}. The microscopic features of the porous SDC scaffolds and the SSC-infiltrated SDC cathodes were characterized using scanning electron microscopes (QUANTA-200, JEOL-S4800). The electrical conductivities were measured in air using the four-probe dc method between 300 °C and 900 °C. The thermal expansion

behavior was observed from 150 °C to 800 °C in air at a heating rate of 5 °C min^{-1} using a Netsch DIL 402 C/S/G dilatometer.

The electrochemical impedance spectra (EIS) under ambient air conditions were measured using an electrochemical workstation consisting of a Solartron 1260A frequency response analyzer and a Solartron 1287 potentiostat to determine the cathode performance and long-term stability of the symmetrical cells. The applied frequency ranged from 0.1 Hz to 100 kHz, and the signal amplitude was 10 mV. The impedance data were collected using ZView 2.9 software.

2.3. Single cell test

The anode-supported fuel cells (Ni-YSZ/YSZ/SSC-infiltrated SDC) were tested at an in-lab SOFCs test station. Each cell with an effective surface area of 0.48 cm^2 was sealed onto a quartz tube using silver paste to form a reactor. The cell was placed inside a furnace and heated to the testing temperature at a heating rate of 5 °C min^{-1}. Humidified hydrogen (3% H_2O) was fed into the anode chamber at a flow rate of 80 mL min^{-1} [STP], while the cathode was simply exposed to an ambient atmosphere. The *I–V* polarization curves were collected using a digital source meter (Keithley 2420) based on a four-probe configuration.

3. Results and discussion

3.1. Phase structure

Complexing agents are known to play an important role in the synthesis of oxides with a desired phase structure at low temperatures via a sol–gel process [15,23]. Fig. 1 displays XRD patterns for the precursors with different complexing agents after firing at 800 °C for 2 h. As shown in Fig. 1, direct decomposition of the nitrate precursors without the application of complexing agents at 800 °C did not yield a phase-pure SSC perovskite. In the presence of citric acid or urea as a complexing agent, some impurities were still detected after firing under the same conditions. Previous work showed that both citric acid and urea could help yield a pure perovskite phase, but it should be noted that the molar ratio of urea to SSC was greater than 10:1 [23]. In this study, a pure perovskite phase of the SSC was successfully formed by applying glycine as the complexing agent at the relatively low glycine to SSC molar ratio of 2:1. The target loading of the infiltrated SSC could be reached more efficiently if the quantity of the complexing agent is substantially decreased. In addition, a large amount of gaseous products which may have a detrimental effect on the mechanical stability of the scaffold during the subsequent sintering could be avoided by adding a small amount of the complexing agent. Thus, glycine was selected as the complexing agent in this study.

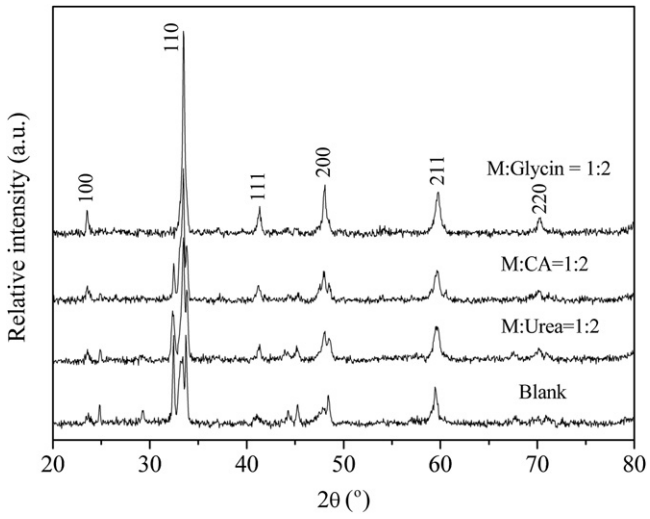

Fig. 1. XRD patterns of the precursors with different complexing agents after firing at 800 °C for 2 h, 'M:complexing agent' indicates the molar ratio of the total metal ions to the complexing agent.

3.2. Microstructure of the scaffold

Porosity and stability of the scaffolds are critical to the preparation of a high-performance cathode by infiltration. These properties were controlled primarily by the firing temperature of the scaffold during the fabrication. A low firing temperature will lead to the high porosity that is beneficial for gas diffusion, while a high firing temperature can ensure the good connection of the scaffold particles that is efficient for oxygen ion transport. The optimal fabrication temperature is a trade-off of the above two factors. The firing temperature of the Gd-doped ceria above 1300 °C reportedly resulted in large cathode polarization resistance [24]. A low firing temperature was also found to decrease the mechanical strength of the scaffold, which could collapse during the infiltration process. Therefore, as a compromise between the porosity and the connectivity of the scaffold, a firing temperature of 1300 °C was selected for fabricating the scaffold layer in this study. Fig. 2a shows a typical cross-sectional view of an SDC scaffold fired at 1300 °C. The adhesion between the scaffold layer and electrolyte layer was found to be acceptable. However, the porosity was relatively low, only ~35%, as determined using the Archimedes method. The infiltration of perovskite oxides into the pores of the scaffolds will inevitably lead to a further decrease in porosity such that the porosity is insufficient. In this research, polyvinyl butyral (PVB), soluble starch and graphite spheres were investigated as pore formers to increase the porosity. Fig. 2b–d provides typical cross-sectional views of the SDC scaffolds with the addition of different pore formers (10 wt%). As expected, good adhesion between the scaffold layer and the electrolyte layer was maintained for all samples after the addition of the pore formers. However, the microstructure and porosity of the scaffolds clearly differed among the different pore formers. The particle sizes of the SDC increased after the introduction of the pore formers, an observation that may be related to the special morphology of the pore formers and the exothermal nature for the elimination of the pore formers during oxidation [25]. When graphite was applied as the pore former, finding pores in the cathode becomes difficult, which suggests that graphite was not a good pore former for the preparation of porous SDC scaffolds. Pores of large size and with relatively well-distributed particles were found when PVB was applied as the pore former, while particles of uniformly distributed size and smaller pores were observed when soluble starch was applied as the pore former. Based on the analysis of a series of SEM micrographs, the porous SDC prepared using 10 wt% PVB as the pore former had a porosity of ~50%, which is ideal for solution infiltration. Thus, through subsequent investigations, PVB was selected as the primary pore former.

3.3. Electrical conductivity

Fig. 3 shows the electrical conductivity from 300 to 900 °C for the SSC-infiltrated SDC with differing amounts of SSC in the porous SDC bars. The electrical conductivities at 700 °C were 0.2, 0.4 and 15 S cm^{-1} for the cathodes containing 10, 15 and 20 wt% SSC, respectively. The relatively low conductivities of the samples with 10 and 15 wt% SSC suggested that the infiltrated SSC particles did

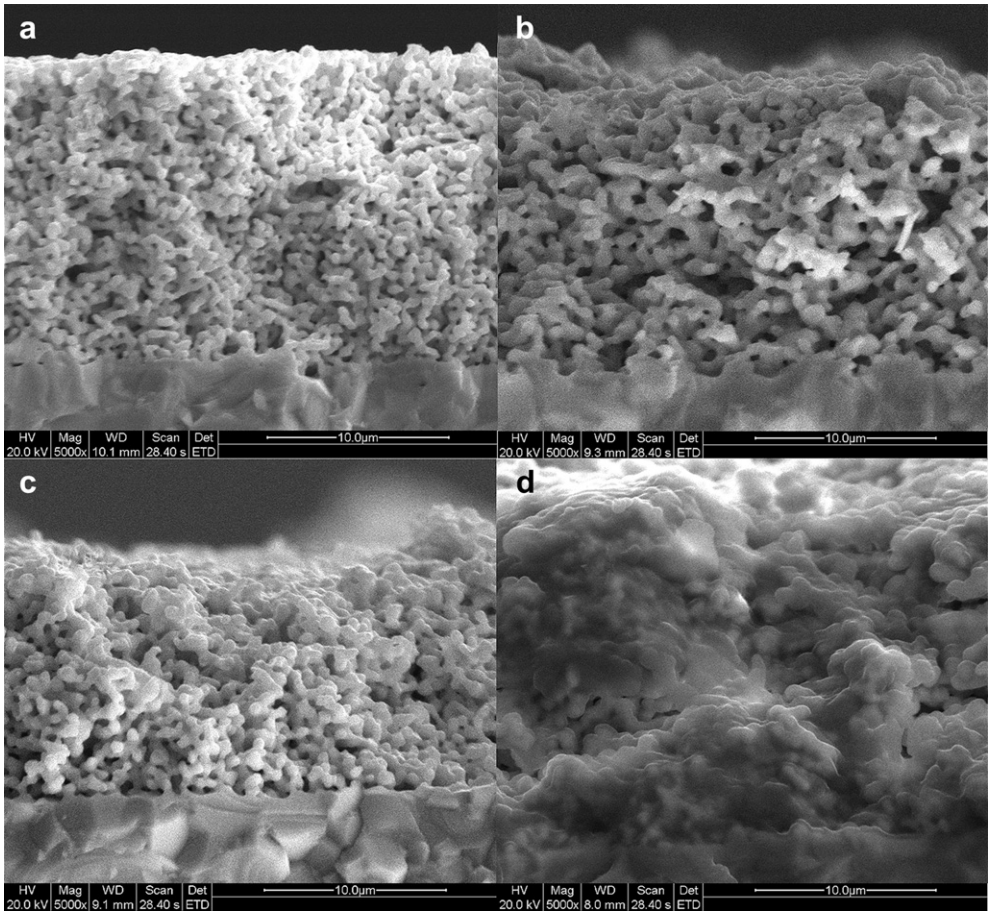

Fig. 2. Typical SEM micrographs of a cross-sectional view of the SDC scaffold fired at 1300 °C without a pore former (a), with PVB (b), with soluble starch (c) and with graphite (d).

not form a well-connected network. After infiltration of the 20 wt% SSC, the conductivities increased dramatically, suggesting that a continuous network of SSC particles was formed. Similar behavior was previously observed for an LSC-infiltrated YSZ cathode [17]; in that study, a dramatically increased conductivity of percolation of the LSC phase was achieved at an LSC content of 30 wt%. The electrical conductivity of the 20 wt% SSC-infiltrated SDC cathode in this study was even higher than that of the 30 wt% LSC-infiltrated YSZ cathode reported by Gorte et al. [17]. This difference may be due to a more uniform distribution of the SSC particles inside the SDC scaffold from the addition of ethanol during fabrication in the current study and from the higher conductivity of SSC over that of LSC. Liu et al. reported that ethanol can improve the wettability of LSCF grains [23]. Although the apparent electrical conductivity of the as-prepared SSC-infiltrated SDC cathodes is still much lower than that of a pure dense SSC (with a maximum conductivity higher than 2000 S cm^{-1}), previous reports have proven that the relatively low conductivity of such porous cathodes did not obviously affect the cathode performance [17]. In addition, the electrical conductivity was not the only factor determining the cathode performance for infiltrated cathodes; thus, the highest electrical conductivity did not necessarily lead to the highest cathode performance [26].

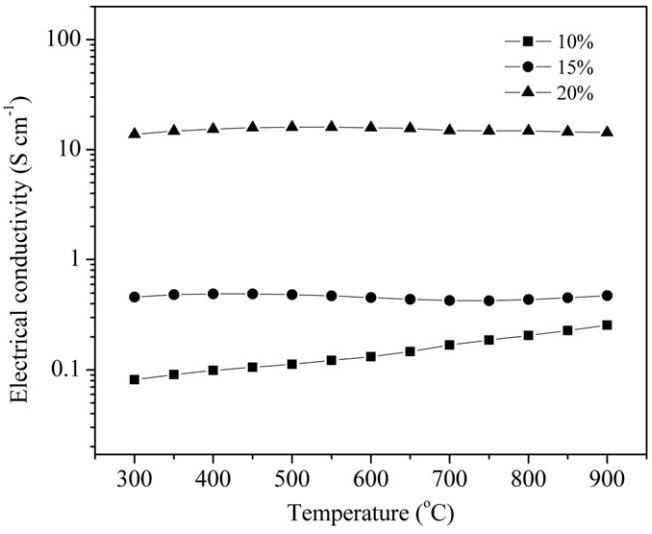

Fig. 3. Electrical conductivities of the SDC bars infiltrated with varying amounts of SSC.

3.4. Thermal expansion behavior

As previously mentioned, the thermal expansion mismatch of cell components is one of the most important issues. Fig. 4 shows the thermal expansion curves measured between 150 °C and 850 °C for porous SDC bars (~50%) with and without infiltration of 20 wt% SSC perovskite oxide. The TEC of the porous SDC was 12.74×10^{-6} K^{-1}, which was almost identical to the value of the dense SDC. The TEC increased only slightly to 13.28×10^{-6} K^{-1} following the introduction of 20 wt% SSC into the SDC scaffold by infiltration. The TEC of 55 wt% LSC-infiltrated YSZ has also been

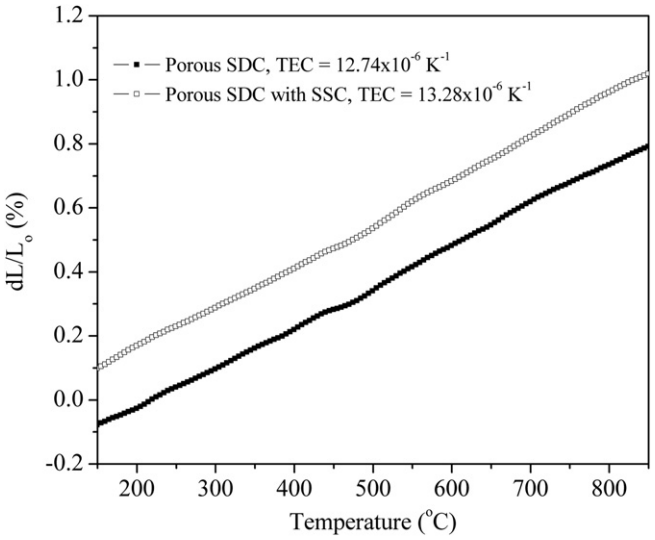

Fig. 4. Thermal expansion behavior of porous SDC bars with and without infiltration of SSC.

reported as only 12.6×10^{-6} K^{-1} [17]. This result can be explained by the fact that the thermal expansion of those infiltrated composites was primarily determined by the porous scaffold, while for the conventional composite cathodes, the TEC is dependent on the weight (volume) ratio of each component. The similarity between the thermal expansion behavior of the infiltrated cathodes and the scaffold ensures the long-term stability of the fuel cell because, typically, the same or similar scaffold material is applied as the electrolyte.

3.5. Microstructure following infiltration

A typical cross-sectional microstructure of the infiltrated cathode with 20 wt% SSC was characterized by SEM and is shown in Fig. 5a. Well-connected particles of ~100 nm diameter were found to coat the inner surface of the porous SDC scaffold firmly and uniformly. The formation of a uniformly continuous network was related not only to the use of ethanol but also to the use of glycine as the complexing agent. Recently, a similar phenomenon was observed by infiltrating $PrBaCo_2O_5$ into a porous SDC scaffold by adding glycine [27]. This relatively large SSC particle size (~100 nm) was actually beneficial for achieving long-term operational stability because smaller particles were less stable at elevated temperatures [21]. The stable particulate morphology of the infiltrated SSC was clearly shown in a comparison of the SEM images of the fresh cathode with the infiltrated SSC (Fig. 5a) and the cathode after a long-term stability test at 700 °C for 200 h (Fig. 5b). Similar morphology and SSC particle size were demonstrated in the cathodes before and after the long-term stability test. It seems that the particle growth was suppressed because the SSC particle size was relatively large (~100 nm) and the stacking of SSC particles was quasi-two-dimensional on the surface of SDC scaffold. The phenomenon of suppressed particle growth has also been previously observed on the $La_{0.6}Sr_{0.4}Co_{0.2}Fe_{0.8}O_{3-\delta}$ cathode infiltrated into the YSZ scaffold [28] and the $Y_{0.5}Bi_{1.5}O_3$ cathode infiltrated into the $La_{0.85}Sr_{0.15}MnO_{3-\delta}$ scaffold [29].

3.6. Electrochemical performance

The electrochemical performance of the 20 wt% SSC-infiltrated SDC composite as an SOFCs cathode was first tested in a symmetrical cell configuration using EIS. Fig. 6 shows two typical impedance spectra collected from the symmetrical cells, which were measured in air under open circuit conditions at 650 and 600 °C. To simultaneously show the two impedance spectra obtained at different operating temperatures, the curves belonging to the electrical inductance process were cut, and the impedance resistances of the electrolyte were removed. The cathode polarization resistance (R_p), calculated from the difference between the real axis intercepts of the spectra in the Nyquist plot, is directly related to the oxygen reduction activity of the cathode. In the Nyquist plot, a depressed arc was observed, which could be separated into two arcs. The high-frequency arc was believed to correspond to the charge transfer process, while the low-frequency arc was probably associated with a non-charge-transfer process [30]. This finding suggests that the infiltrated cathode has similar rate-determining steps to those of a cathode prepared by the traditional co-firing method. As shown in the inset of Fig. 6, R_p values of 0.05, 0.09, 0.19 and 0.51 Ω cm^2 at 700, 650, 600 and 550 °C, respectively, were plotted according to the Arrhenius equation. The R_p values of the SSC-infiltrated SDC are lower than those of the conventional composite cathodes prepared by co-firing of pre-mixed powders. For example, a co-fired SSC + SDC cathode had an R_p of approximately 0.3 Ω cm^2 at 600 °C [31]. An even larger R_p value of approximately 0.6 Ω cm^2 was obtained by co-firing an $L_{0.58}$SCF + GDC cathode at 1000 °C and testing it at 650 °C [32]. In addition, at 600 °C, the present R_p was comparable with that of similar LSC cathodes or SSC infiltrated into ceria-based electrolyte scaffolds [15,33]. The results indicated that 20 wt% SSC in the composite layer is sufficient to achieve an acceptable polarization resistance for fuel cell operation. In addition, as shown in Fig. 6, the activation energy (E_a) for the oxygen reduction over the SSC-

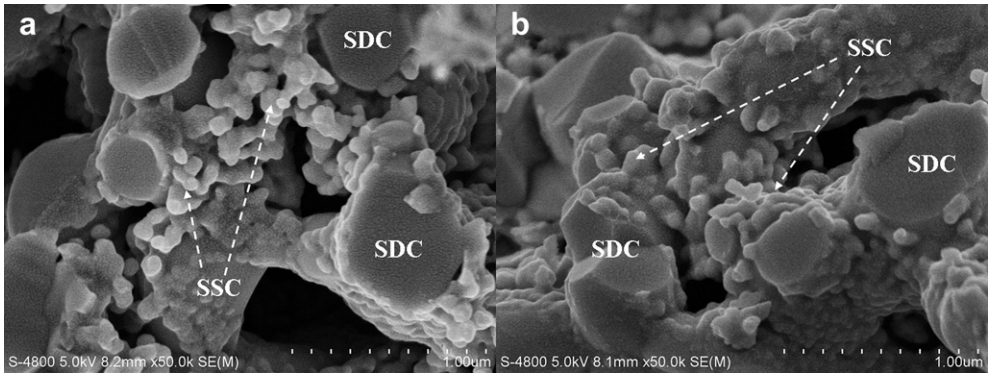

Fig. 5. Typical cross-sectional microstructure of the infiltrated cathode with 20 wt% SSC prior to (a) and after a long-term stability test (b).

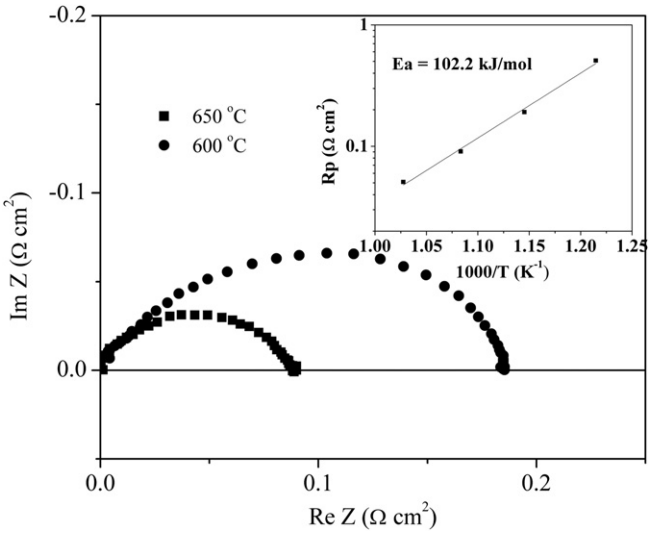

Fig. 6. Cathode polarization resistances of the 20 wt% SSC-infiltrated SDC composite cathode at different operating temperatures and the two typical impedance spectra measured in air under open-circuit conditions at 650 and 600 °C.

infiltrated SDC cathode, calculated from the temperature dependence of the R_p, is 102.2 kJ mol^{-1}. The low E_a and R_p values derived from the symmetrical cells indicate that the SSC-infiltrated SDC cathode can maintain high activity for ORR at intermediate temperatures.

To further confirm the oxygen reduction activity, the electrochemical performance of the SSC-infiltrated SDC cathode was investigated using single cells with a Ni-YSZ anode and a thin-film YSZ electrolyte (15 μm). Fig. 7 presents the *I–V* and *I–P* curves of a single cell operating at various temperatures. The open circuit voltage (OCV) was 1.08 V at 750 °C and increased with a decrease in the operating temperature. The OCVs of the single cell with the thin-film electrolyte are close to the theoretical values, suggesting a perfect sealing of cells and a well-densified electrolyte structure. The linear *I–V* curves indicate that no concentration polarization occurred in the fuel cells, even at a high polarization current density. This result implies that the porosity of the optimized scaffold is sufficient even after infiltrating with up to 20 wt% SSC. Peak power densities (PPDs) of 1205, 936, 624 and 378 mW cm^{-2} were achieved at 750, 700, 650 and 600 °C, respectively. As expected, these power densities are higher than those of single cells with SSC-based cathodes and zirconia-based electrolytes. Our results are also higher than those found in the literature for a similar cell. For example, a PPD of only 660 mW cm^{-2} was achieved at 700 °C with 10-μm-thick ScSZ electrolyte and an SSC-infiltrated cathode [34].

The long-term stability of an infiltrated cathode at elevated temperatures is a major concern for practical applications [28,35]. It has been proposed that the growth and coalescence of the nanosized particles and the phase reaction between the nanosized particles and scaffold may be responsible for the performance degradation [28,35]. The electrochemical performance durability of the SSC-infiltrated SDC cathode was also measured at 700 °C for approximately 300 h. During the measurement, an Ag-mesh was adopted as the current collector to minimize the contribution of the current collector to the performance stability of the cathode [36]. As shown in Fig. 8a, the polarization resistance of the SSC-infiltrated SDC cathode was stable at ∼0.14 Ω cm^2 within the test period of approximately 300 h. The impedance spectra of the symmetrical cell both before and after the 300 h test period are shown in Fig. 8b. Two impedance spectra can almost overlap with no degradation, which further indicates their excellent stability under this test condition. In connection with the SEM images in

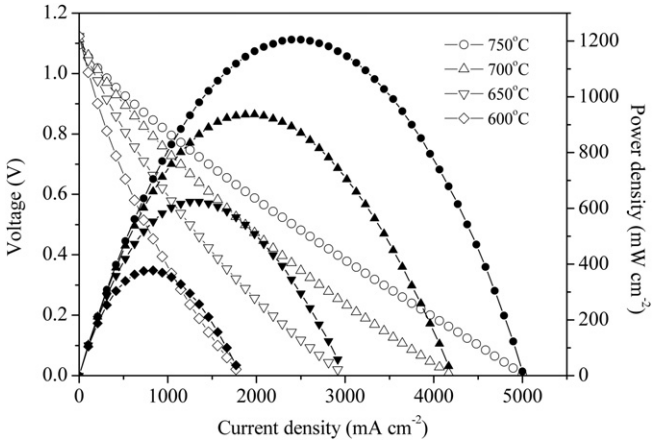

Fig. 7. *I–V* and *I–P* curves of the single cell with a 20 wt% SSC-infiltrated SDC cathode, a Ni-YSZ anode and a thin-film YSZ electrolyte (15 μm).

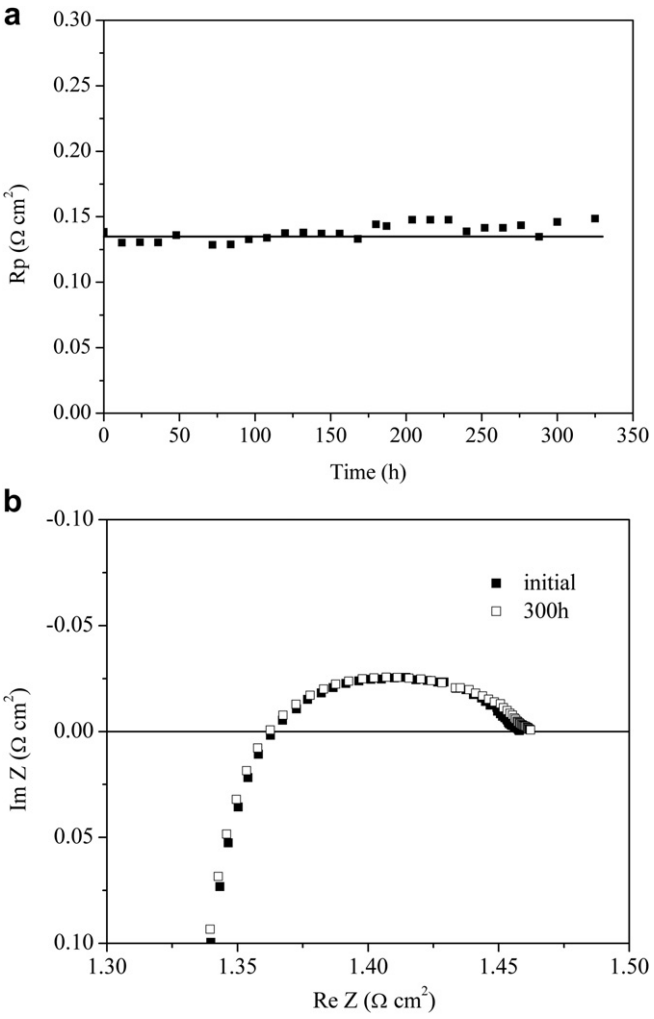

Fig. 8. Time dependence of the polarization resistances of the 20 wt% SSC-infiltrated SDC cathode at 700 °C (a) and the corresponding electrochemical impedance spectra measured before and after operation over 300 h (b).

Fig. 5, the high operational stability is closely related to the high morphological stability of the submicron infiltrated SSC particles in the cathode and the negligible phase reaction between the infiltrated SSC particles and SDC scaffold.

In addition to the infiltration of SSC into the porous SDC scaffold to perform as a cathode of SOFCs, SSC may also be infiltrated into a YSZ scaffold because the phase reaction between SSC and YSZ is low at the sintering temperature of 800 °C. Attractive initial cathode polarization resistances of 0.031, 0.057, 0.104, 0.200 and 0.541 Ω cm^2 were achieved at 800, 750, 700, 650 and 600 °C, respectively. These results are comparable to those of symmetrical cells prepared by the infiltration of LSC into porous YSZ scaffolds (0.12 Ω cm^2 at 700 °C) [17] and $La_{0.8}Sr_{0.2}FeO_{3-\delta}$ into porous YSZ scaffolds (0.1 Ω cm^2 at 700 °C) [37] as reported in the literature. Though SSC particles were proved to be stable according to the typical SEM images in Fig. 5, the long-term operation of such a cathode is still questionable. The phase reaction between cobalt-containing perovskite oxides and YSZ electrolyte at elevated temperatures was widely demonstrated and the reaction between SSC and YSZ was also thermodynamically favored. To demonstrate whether such an infiltrated cathode can be operated stably for an extended time, the stability of a similar SSC-infiltrated YSZ cathode was evaluated. As shown in Fig. 9, an obvious gradual increase in the cathode polarization resistance was observed as a function of the operating time during the 325 h test. To detect the potential reaction between the YSZ and SSC, the solid reaction between them in powder formation was first conducted. As shown in Fig. 10, the insulating phases could not be observed after firing the SSC and YSZ powders at 700 °C for 200 h, and all diffraction peaks could still be assigned to a mixture of the SSC and YSZ phases. Considering that the degree and activity between the submicron particles and the scaffold are quite different from those of traditional micro-sized powders, the XRD of the SSC-infiltrated YSZ cathode after firing at 700 °C for 200 h was characterized by the results shown in Fig. 10. For comparison, the XRD patterns of a fresh SSC-infiltrated YSZ sample are also shown in Fig. 10. The diffraction peaks assignable to the insulating $SrZrO_3$ and $Sm_2Zr_2O_7$ phases appeared after the firing at 700 °C for 200 h, suggesting the existence of a solid-phase reaction between the SSC and YSZ under these conditions. Some unknown diffraction peaks also appeared, and one diffraction peak characteristic of the SSC phase disappeared.

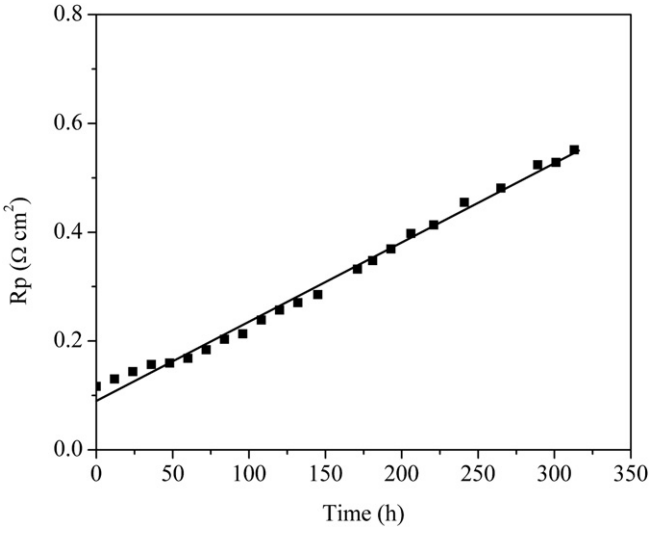

Fig. 9. Time dependence of the polarization resistances of the 20 wt% SSC-infiltrated YSZ cathode at 700 °C.

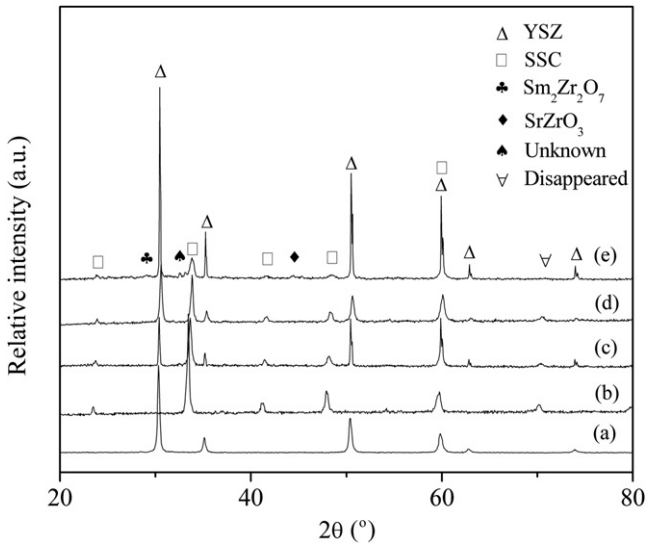

Fig. 10. XRD patterns of fresh YSZ (a), fresh SSC (b), fresh SSC-infiltrated YSZ composite (c), SSC + YSZ powders after firing at 700 °C for 200 h (d) and SSC-infiltrated YSZ composite after firing at 700 °C for 200 h (e).

The strongest diffraction peak of the $SrZrO_3$ phase was not detected in this experiment, suggesting that the $SrZrO_3$ phase had a specific crystalline orientation. Based on these XRD results, it was clear that although the infiltration of SSC into the YSZ scaffold may decrease the firing temperature below the obvious phase reaction for the conventional powder, the interfacial reaction between the SSC and YSZ in the cathode is unavoidable at the given operating temperature over an extended period. To overcome this drawback, an SDC scaffold is preferred to avoid the phase reaction within the cathode; in addition, the scaffold could also act as a diffusion barrier, avoiding direct contact between the SSC in the cathode and the YSZ electrolyte and ensuring high operational stability.

4. Conclusions

$Sm_{0.5}Sr_{0.5}CoO_{3-\delta}$-infiltrated cathodes for SOFCs with improved ORR activity and stability were successfully fabricated. Complexing agents were found to be important for deriving a pure perovskite, and a phase-pure SSC was obtained after heating at 800 °C with the addition of glycine as the complexing agent at a relatively low glycine content. The microstructures of the scaffold were closely related to the pore formers, and PVB was selected as the pore former for fabricating a porous scaffold. The infiltration of 20 wt% SSC into the SDC scaffold only slightly increased the TEC to 13.28×10^{-6} K^{-1}, a value similar to that of the SDC scaffold, suggesting that the TEC of the infiltrated composite was primarily determined by the scaffold. An electrical conductivity 15 S cm^{-1} was achieved at 700 °C, indicating that well-connected SSC particles were formed with the 20 wt% SSC + 80 wt% SDC. This result was further supported by the SEM results. By infiltrating 20 wt% SSC into a porous SDC scaffold, a low cathode polarization resistance of 0.05 Ω cm^2, a high peak power density of 936 mW cm^{-2} and a stable performance over 325 h of operation at 700 °C were achieved, suggesting that the SSC-infiltrated SDC cathodes were suitable for practical application. However, with the SSC infiltrated into a porous YSZ scaffold, the interfacial reaction between the SSC and YSZ was still occurring over the long-term operation at 700 °C and led to a gradual increase in the cathode polarization resistance. Therefore, SDC was preferred as a porous scaffold for the infiltration of SSC to ensure long-term operational stability.

Acknowledgments

This work was supported by the "National Science Foundation for Distinguished Young Scholars of China" under contract No. 51025209.

References

[1] A.B. Stambouli, E. Traversa, Renew. Sustain. Energy Rev. 6 (2002) 433–455.
[2] B.C.H. Steele, A. Heinzel, Nature 414 (2001) 345–352.
[3] E.D. Wachsman, K.T. Lee, Science 334 (2011) 935–939.
[4] C.S. Ding, T. Hashida, Energy Environ. Sci. 3 (2010) 1729–1731.
[5] C.W. Sun, R. Hui, J. Roller, J. Solid State Electrochem. 14 (2010) 1125–1144.
[6] F.F. Dong, D.J. Chen, R. Ran, H. Park, C. Kwak, Z.P. Shao, Int. J. Hydrogen Energy 37 (2012) 4377–4387.
[7] H. Fukunaga, M. Koyama, N. Takahashi, C. Wen, K. Yamada, Solid State Ionics 132 (2000) 279–285.
[8] Y.M. Guo, D.J. Chen, H.G. Shi, R. Ran, Z.P. Shao, Electrochim. Acta 56 (2011) 2870–2876.
[9] T. Hibino, A. Hashimoto, T. Inoue, J.I. Tokuno, S.I. Yoshida, M. Sano, Science 288 (2000) 2031–2033.
[10] L. Yang, C.D. Zuo, S.Z. Wang, Z. Cheng, M.L. Liu, Adv. Mater. 20 (2008) 3280–3283.
[11] C.R. Xia, W. Rauch, F.L. Chen, M.L. Liu, Solid State Ionics 149 (2002) 11–19.
[12] X.G. Zhang, M. Robertson, S. Yick, C. Deces-Petit, E. Styles, W. Qu, Y.S. Xie, R. Hui, J. Roller, O. Kesler, R. Maric, D. Ghosh, J. Power Sources 160 (2006) 1211–1216.
[13] D. Skarmoutsos, F. Tietz, P. Nikolopoulos, Fuel Cells 1 (2001) 243–248.
[14] D.J. Chen, R. Ran, Z.P. Shao, J. Power Sources 195 (2010) 7187–7195.
[15] F. Zhao, R.R. Peng, C.R. Xia, Fuel Cells Bull. 2008 (2008) 12–16.
[16] S.P. Jiang, Int. J. Hydrogen Energy 37 (2012) 449–470.
[17] Y.Y. Huang, K. Ahn, J.M. Vohs, R.J. Gorte, J. Electrochem. Soc. 151 (2004) A1592–A1597.
[18] X. Xu, F.Z. Wang, Y.H. Liu, J. Pu, B. Chi, L. Jian, J. Power Sources 196 (2011) 9365–9368.
[19] J.M. Vohs, R.J. Gorte, Adv. Mater. 21 (2009) 943–956.
[20] T.Z. Sholklapper, H. Kurokawa, C.P. Jacobson, S.J. Visco, L.C.D. Jonghe, Nano Lett. 7 (2007) 2136–2141.
[21] M. Shah, P.W. Voorhees, S.A. Barnett, Solid State Ionics 187 (2011) 64–67.
[22] D.J. Chen, R. Ran, Z.P. Shao, J. Power Sources 195 (2010) 4667–4675.
[23] X.Y. Lou, Z. Liu, S.Z. Wang, Y.H. Xiu, C.P. Wong, M.L. Liu, J. Power Sources 195 (2010) 419–424.
[24] M. Shah, S.A. Barnett, Solid State Ionics 179 (2008) 2059–2064.
[25] L.F. Nie, J.C. Liu, Y.J. Zhang, M.L. Liu, J. Power Sources 196 (2011) 9975–9979.
[26] S. Choi, J. Shin, G. Kim, J. Power Sources 201 (2012) 10–17.
[27] Y. Wang, H. Zhang, F.L. Chen, C.R. Xia, J. Power Sources 203 (2012) 34–41.
[28] Y.H. Liu, B. Chi, J. Pu, J. Li, Int. J. Hydrogen Energy 37 (2012) 4388–4393.
[29] Z.Y. Jiang, C.R. Xia, F. Zhao, F.L. Chen, Electrochem. Solid State Lett. 12 (2009) B91–B93.
[30] S.B. Adler, Chem. Rev. 104 (2004) 4791–4843.
[31] S.W. Baek, C. Lee, J. Bae, J. Fuel Cell Sci. Technol. 6 (2009) 031010-1–031010-5.
[32] F. Qiang, K.N. Sun, N.Q. Zhang, X.D. Zhu, S.R. Le, D.R. Zhou, J. Power Sources 168 (2007) 338–345.
[33] J.D. Nicholas, S.A. Barnett, J. Electrochem. Soc. 157 (2010) B536–B541.
[34] H. Zhang, F. Zhao, F.L. Chen, C.R. Xia, Solid State Ionics 192 (2011) 591–594.
[35] J. Chen, F.L. Liang, D. Yan, J. Pu, B. Chi, S.P. Jiang, L. Jian, J. Power Sources 195 (2010) 5201–5205.
[36] Y.B. Chen, F.C. Wang, D.J. Chen, F.F. Dong, H.J. Park, C. Kwak, Z.P. Shao, J. Power Sources 210 (2012) 146–153.
[37] Y.Y. Huang, J.M. Vohs, R.J. Gorte, J. Electrochem. Soc. 151 (2004) A646–A651.